ARTICLE
Journal of Cellular Biochemistry 117:2302–2314 (2016)

Journal of Cellular Biochemistry

Moringa oleifera Gold Nanoparticles Modulate Oncogenes, Tumor Suppressor Genes, and Caspase-9 Splice Variants in A549 Cells

Charlette Tiloke,[1] Alisa Phulukdaree,[1,2] Krishnan Anand,[3] Robert M. Gengan,[3] and Anil A. Chuturgoon[1]*

[1]*Discipline of Medical Biochemistry and Chemical Pathology, School of Laboratory Medicine and Medical Sciences, College of Health Sciences, University of KwaZulu-Natal, Congella, Durban 4013, South Africa*

[2]*Department of Physiology, School of Medicine, Faculty of Health Sciences, University of Pretoria, Pretoria, South Africa*

[3]*Department of Chemistry, Faculty of Applied Sciences, Durban University of Technology, Durban 4001, South Africa*

ABSTRACT

Gold nanoparticles (AuNP's) facilitate cancer cell recognition and can be manufactured by green synthesis using nutrient rich medicinal plants such as *Moringa oleifera* (MO). Targeting dysregulated oncogenes and tumor suppressor genes is crucial for cancer therapeutics. We investigated the antiproliferative effects of AuNP synthesized from MO aqueous leaf extracts (ML_{AuNP}) in A549 lung and SNO oesophageal cancer cells. A one-pot green synthesis technique was used to synthesise ML_{AuNP}. A549, SNO cancer cells and normal peripheral blood mononuclear cells (PBMCs) were exposed to ML_{AuNP} and C_{AuNP} to evaluate cytotoxicity (MTT assay); apoptosis was measured by phosphatidylserine (PS) externalization, mitochondrial depolarization ($\Delta\Psi m$) (flow cytometry), caspase-3/7, −9 activity, and ATP levels (luminometry). The mRNA expression of *c-myc*, *p53*, *Skp2*, *Fbw7*α, and *caspase-9* splice variants was determined using qPCR, while relative protein expression of c-myc, p53, SRp30a, Bax, Bcl-2, Smac/DIABLO, Hsp70, and PARP-1 were determined by Western blotting. ML_{AuNP} and C_{AuNP} were not cytotoxic to PBMCs, whilst its pro-apoptotic properties were confirmed in A549 and SNO cells. ML_{AuNP} significantly increased caspase activity in SNO cells while ML_{AuNP} significantly increased PS externalization, $\Delta\Psi m$, caspase-9, caspase-3/7 activities, and decreased ATP levels in A549 cells. Also, p53 mRNA and protein levels, SRp30a ($P = 0.428$), Bax, Smac/DIABLO and PARP-1 24 kDa fragment levels were significantly increased. Conversely, ML_{AuNP} significantly decreased Bcl-2, Hsp70, Skp2, Fbw7α, *c-myc* mRNA, and protein levels and activated alternate splicing with *caspase-9a* splice variant being significantly increased. ML_{AuNP} possesses antiproliferative properties and induced apoptosis in A549 cells by activating alternate splicing of *caspase-9*. J. Cell. Biochem. 117: 2302–2314, 2016.

KEY WORDS: GOLD NANOPARTICLES; *MORINGA OLEIFERA*; LUNG CANCER; c-myc; SPLICE VARIANTS; APOPTOSIS

Cancer is the second leading cause of mortality worldwide following cardiovascular disease with approximately 8.2 million cancer deaths (21.7% of noncommunicable diseases) and 14.1 million new diagnoses [Globocan, 2012; Mendis et al., 2014]. Cancer mortality is projected to increase to 12.6 million by year 2030. Lung cancer alone accounts for 1.59 million deaths and is the leading cause of cancer mortality [Globocan, 2012]. Despite major advancements in cancer therapies, it remains incurable and quality of life after diagnosis is reduced [Cheng et al., 2005]. Bello et al. [2011] suggested South Africans are at higher risk of developing lung cancer due to their lifestyle changes and the high burden of infectious diseases [Bello et al., 2011].

Cancer cells are able to proliferate through activation of oncogenes (e.g., c-myc) and inactivation of tumor suppressor genes (e.g., p53) [Bonomi et al., 2013]. Oncogenes and dysregulation of tumor suppressor genes encourage tumor progression. Apoptosis

Conflicts of interest: The authors declare that they have no conflict of interest.

Grant sponsor: National Research Foundation, South Africa; Grant sponsor: University of KwaZulu-Natal College of Health Sciences.

*Correspondence to: Prof. Anil A. Chuturgoon, Discipline of Medical Biochemistry and Chemical Pathology, School of Laboratory Medicine and Medical Sciences, College of Health Sciences, University of KwaZulu-Natal, Private Bag 7, Congella, Durban 4013, South Africa. E-mail: chutur@ukzn.ac.za

Manuscript Received: 21 July 2015; Manuscript Accepted: 25 February 2016

Accepted manuscript online in Wiley Online Library (wileyonlinelibrary.com): 29 February 2016

DOI 10.1002/jcb.25528 • © 2016 Wiley Periodicals, Inc.

maintains homeostasis and any disruption to this process leads to cancer pathogenesis. c-Myc, a transcription factor, regulates gene expression for cell growth and apoptosis [Chen et al., 2013], while Skp2 (S-phase kinase-associated protein 2) and Fbw7 (F-box and WD repeat domain-containing 7) mediate the posttranslational regulation of c-myc. Skp2 also acts as an oncogene and is overexpressed in human cancers [Chen et al., 2013].

Cancer cells metabolic activity are increased enabling them to rapidly divide [Eblen, 2012]. Chemotherapeutic agents are non-specific as they target these rapidly dividing cells at the expense of normal healthy cells [Eblen, 2012]. Differential expression of genes and proteins are seen in chemotherapy resistance. The cellular proteome is a key regulator in chemotherapy. Fundamental processes such as gene expression, mRNA transcription and translation into protein as well as modification and degradation of proteins influence the cellular proteome. In particular, alternate splicing of pre-mRNA also affects the cellular proteome as it determines which variant of the gene is translated, resulting in proteins with differing functional efficacy. For example, the splice variant of *caspase-9* has shown that expression of *caspase-9b* inhibits apoptosis and is implicated in chemotherapy resistance [Shultz et al., 2011]. On the other hand, *caspase-9a* expression induces apoptosis and thus regulation of inclusion/exclusion of exon 3, 4, 5, and 6 cassette is a determinant of cell fate. This process is often manipulated by cancer cells to ensure their survival [Eblen, 2012].

Emerging cancer therapies such as nanoparticles (NP′s) are now being developed to specifically target cancer cells [Zhang et al., 2003]. Nanoparticles have characteristic properties of being very small (1–100 nm) [Kumar et al., 2011] and are able to interact with biomolecules both on the cell surface and intracellularly [Cai et al., 2008]. Nanoparticles are useful in anticancer drug delivery systems, however, their exact mechanism of action still remains to be elucidated [Kang et al., 2010]. Among the many nanoparticles being developed, studies show that gold nanoparticles (AuNP′s) are stable and can easily enter a cell, and are useful in the treatment of rheumatoid arthritis, possess anticancer and antimicrobial properties, and have good biocompatibility [Tedesco et al., 2010; Kumar et al., 2011; Siddiqi et al., 2012]. Gold nanoparticles also have therapeutic potential as an anti-HIV agent [Kumar et al., 2011]. The advantage of AuNP′s is that they are biologically inert and non-toxic [Lim et al., 2011; Parveen and Roa, 2014] and their use is favored over toxic silver and cadmium nanoparticles that are commercially in demand. Nanoparticle properties and applications are due to their size and shape [Xie et al., 2007b, 2009]. Nanoparticles are synthesized chemically or via the use of medicinal plants [Prasad and Elumalai, 2011]. In addition, NP′s can be synthesized using biological extracts such as green algae and bovine serum albumin [Xie et al., 2007a,c]. The use of plant extracts to synthesize nanoparticles is recently discovered [Prasad and Elumalai, 2011] and this green chemistry is cost effective and advantageous in large scale production, especially in third world countries [Salamanca-Buentello et al., 2005].

Moringa oleifera (MO) belongs to the family Moringaceae, commonly known as Drumstick tree [Fahey, 2005; Goyal et al., 2007], is indigenous to India and is also found widely in South Africa (SA). Almost all parts of the tree possess medicinal properties however the leaves contain high nutritional source of vitamins, calcium, iron, potassium, proteins and possess antioxidant, anticancer and hepatoprotective properties [Prasad and Elumalai, 2011; Sreelatha et al., 2011]. Due to SA′s socio-economic, cultural background, and minimal support of basic healthcare in rural areas, MO has been widely used for the treatment and management of malnutrition, diabetes mellitus, cardiovascular and liver diseases among several others [Erasto et al., 2005; Goyal et al., 2007]. The leaf extract contain bioactive compounds which aid in its anticancer activity. These compounds include niazimicin, gallic acid, rhamnose, glucosinolates, and isothiocyanates [Fahey, 2005; Goyal et al., 2007; Mishra et al., 2011]. Recently, AuNP′s of MO flower petals were prepared and showed activity in A549 lung cancer cells [Anand et al., 2014]. Our study now is on the leaf extract which was used in an environmentally friendly synthesis of AuNP′s (ML_{AuNP}). We investigated the antiproliferative and apoptosis inducing effects of a novel ML_{AuNP} in cancerous A549 lung cells. It was hypothesized that ML_{AuNP} has an antiproliferative effect by inducing apoptosis in A549 cells as a result of ML_{AuNP} selectively targeting oncogenes and tumor suppressor genes.

MATERIALS AND METHODS

MATERIALS

Moringa oleifera leaves were collected from the KwaZulu-Natal region (Durban, SA) and verified by the KwaZulu-Natal (SA) herbarium (Batch no. CT/1/2012, Genus no. 3128). Gold (III) chloride trihydrate ($HAuCl_4.3H_20$) was purchased from Sigma–Aldrich, SA. A549 cells were purchased from Highveld Biologicals (Johannesburg, SA). Cell culture reagents were purchased from Whitehead Scientific (Johannesburg, SA). ECL-LumiGlo® chemiluminescent substrate kit was purchased from Gaithersburg and Western blot reagents were purchased from Bio-Rad. All other reagents were purchased from Merck (SA).

SYNTHESIS OF ML_{AuNP}

A one-pot green synthesis technique was used to synthesise ML_{AuNP} [Anand et al., 2014; Li et al., 2015]. The synthesis and characterization were conducted at Durban University of Technology (Durban, SA). The MO leaf extract was prepared as per Tiloke et al. [2013]. The resultant extract (5 ml) was added to 1 mM aqueous gold chloride solution (100 ml) and allowed to react at room temperature (RT) for the reduction of Au^{3+} ions to Au. ML_{AuNP} were then characterized and particle size was determined using UV spectrometry and transmission electron microscopy, respectively. In addition, further characterization of the hydrodynamic size and size distribution of the ML_{AuNP} was determined using dynamic light scattering (DLS) and Image J. The Zeta potential of ML_{AuNP} was also assessed.

SYNTHESIS OF TRISODIUM CITRATE GOLD NANOPARTICLES (C_{AuNP})—CHEMICAL SYNTHESIS METHOD

The synthesis and characterization were conducted at Durban University of Technology (Durban, SA). A volume of 100 ml Au (III)

(1.4 mM) was used with the addition of 2 ml of 0.34 M trisodium citrate. This was allowed to stir continuously for the production of C_{AuNP}.

PERIPHERAL BLOOD MONONUCLEAR CELL EXTRACTION

Whole blood was obtained from a healthy male donor and the peripheral blood mononuclear cells (PBMCs) were isolated from heparinized whole blood by differential centrifugation (Ethical approval from the University of KwaZulu-Natal Biomedical Research Ethics Committee [Reference number: BE057/15] and informed consent was obtained). Briefly, 5 ml of whole blood was layered onto equivolume Histopaque 1077 (Sigma, Germany) in 15 ml conical tubes and centrifuged (400*g*, 30 min, RT). The buffy coat layer containing PBMCs were aspirated into sterile 15 ml conical tubes and washed twice in 0.1 M phosphate buffered saline (PBS) (400*g*, 10 min). Cell numbers were then enumerated using trypan blue.

CELL CULTURE AND EXPOSURE PROTOCOL

A549 and SNO cells were cultured in 25 cm^3 culture flasks in complete culture media (CCM) comprising of Eagle's minimum essential medium (EMEM) supplemented with 10% foetal calf serum, 1% L-glutamine and 1% penicillin-streptomycin-fungizone [Wilson and Walker, 2005]. Cell growth was monitored and cultures were maintained at 37°C with 5% CO_2. A549 and SNO cells were grown to 90% confluency and treated with the C_{AuNP} and ML_{AuNP}. Isolated PBMCs were cultured at 37°C with 5% CO_2 in Roswell park memorial institute (RPMI) medium 1640 supplemented with 10% foetal calf serum, 1% L-glutamine and 1% penicillin-streptomycin-fungizone [Wilson and Walker, 2005]. Cell density at 20,000 was used per sample in all luminometric and colorimetric assays. A549 cell density at 1,000,000 cells was used for flow cytometric analysis and 2,500,000 cells for western blot and qPCR analysis.

CELL VIABILITY ASSAY

The viability of A549, SNO cells and PBMCs after exposure to C_{AuNP} and ML_{AuNP} was determined using the 3-(4,5-Dimethyl-2-thiazolyl)-2,5-diphenyl-2H-tetrazolium bromide (MTT) assay [Mossman, 1983]. Cells were seeded into a 96-well microtitre plate (20,000 cells/well). The cells were incubated with varying C_{AuNP} concentrations (1.9–475 μg/ml) and ML_{AuNP} concentrations (1.575–393.83 μg/ml) in six replicates (300 μl/well) and incubated (37°C, 5% CO_2) for 24 h. Control cells were incubated with CCM only. A CCM/MTT salt solution (5 mg/ml) was added (120 μl/well) and the plate was incubated (37°C, 4 h). Thereafter, supernatants were removed; dimethyl sulphoxide (DMSO) 100 μl/well was added and incubated (1 h). The optical density of the formazan product was measured (570/690 nm) using a spectrophotometer (Bio-Tek μQuant). The results were expressed as percentage cell viability relative to the control. This experiment was repeated on two separate occasions before the IC_{50} of C_{AuNP} and ML_{AuNP} for the cells (A549, SNO and PBMCs) were determined. Due to minimal toxicity observed in PBMCs, all other experiments were conducted on A549 and SNO cells to determine the mechanism of cell death.

ATP QUANTIFICATION

The CellTitre-Glo® assay (Promega) was used to quantify ATP in samples which is an indication of metabolically active cells. A549 and SNO cells (20,000 cells/well) were seeded into an opaque polystyrene 96-well microtitre plate in six replicates. Following treatment, the CellTiter-Glo® Reagent 2× was prepared according to manufacturer's guidelines and 100 μl of the reagent was added per well. The plate was then incubated in the dark (30 min, RT). Following incubation, the plate was read on the Modulus™ microplate luminometer. The luminescent signal was measured which is proportional to the amount of ATP present and the data was expressed as RLU and fold change.

CASPASE-3/7 AND 9 ACTIVITIES

Caspase-Glo® 3/7 and Caspase-Glo® 9 Assays (Promega) were used to assess apoptosis. For each assay the same procedure was followed: A549 and SNO cells (20,000 cells/well) were seeded into an opaque polystyrene 96-well microtitre plate in six replicates. Following treatment, the Caspase-Glo® 3/7 and Caspase-Glo® 9 reagents were prepared according to manufacturer's guidelines. A volume of 100 μl of the reagent was added per well and incubated in the dark (30 min, RT). Following incubation, the luminescence was measured on a Modulus™ microplate luminometer. The data was expressed as RLU and fold change.

ASSESSMENT OF PHOSPHATIDYLSERINE EXTERNALIZATION

The Annexin-V-Fluos assay (Roche) was used to detect phosphatidylserine (PS) externalization. PS is externalized in both apoptotic and necrotic cells and is therefore differentiated by addition of propidium iodide (PI). PI only stains DNA of necrotic cells. A volume of 100 μl of each sample (1,000,000 cells/tube) were transferred to polystyrene flow cytometry tubes, stained with 100 μl annexin-V-Fluos labeling solution, and incubated in the dark (15 min, RT). A volume of 400 μl of Annexin-V Binding buffer (1×) was added to the samples and the labeled cells were detected by fluorescence-activated cell sorting (FACS) Calibur flow cytometer (BD Biosciences, SA). The cells were gated to exclude cellular debris using FlowJo v7.1 software (Tree Star Inc., Ashland). Approximately 50,000 events were obtained and the data was analyzed using CellQuest PRO v4.02 software (BD Biosciences). The data was expressed as a percentage of apoptotic cells.

MITOCHONDRIAL MEMBRANE POTENTIAL

The JC-1 Mitoscreen assay was used to assess mitochondrial membrane potential according to manufacturers' guidelines. A volume of 100 μl of each sample (1,000,000 cells/tube) was transferred to polystyrene flow cytometry tubes with the addition of 150 μl JC-1 dye and incubated (37°C, 5% CO_2, 10 min). The cells were washed twice with JC-1 wash buffer (1×). Between washes cells were centrifuged (400*g*, 5 min). Cells were re-suspended in 200 μl flow cytometry sheath fluid and labeled cells were detected on FACS Calibur flow cytometer. The cells were gated to exclude cellular debris using FlowJo v7.1 software. 50,000 events were obtained and the data was analyzed using CellQuest PRO v4.02 software. The results were expressed as a percentage of cells containing depolarized mitochondria.

WESTERN BLOTTING

Western Blots were performed to determine the protein levels of c-myc, p53, SRp30a, Bax, Bcl-2, Smac/DIABLO, Hsp70, and PARP-1. Briefly, total protein was isolated using Cytobuster™ reagent supplemented with protease inhibitor (Roche, SA, cat. no. 05892791001) and phosphatase inhibitor (Roche, SA, cat. no. 04906837001). The bicinchoninic acid assay (Sigma, Germany) was used to quantify the protein and was standardized to 1.066 mg/ml [Bainor et al., 2011]. The samples were prepared in Laemmli buffer [Yang and Ma, 2009], boiled (100°C, 5 min) and electrophoresed (150V, 1 h) in 7.5% sodium dodecyl sulfate polyacrylamide gels using a Bio-Rad compact power supply. The separated proteins were electro-transferred to nitrocellulose membrane using the Trans-Blot® Turbo Transfer system (Bio-Rad, SA) (20V, 45 min). The membranes were blocked (1 h) using 3% bovine serum albumin (BSA) in Tris-buffered saline (TTBS—NaCl, KCL, Tris, Tween 20, dH_2O, pH 7.4). Thereafter, the membranes were immune-probed with primary antibody (p53 [ab26], PARP-1 [ab110915], 1:1,500; c-myc [Cell Signaling #9402], SRp30a [PA5-30220], Bax [ab5714], Bcl-2 [Cell Signaling #3869], Hsp70 [BD610607], 1:1,000; and Smac/DIABLO [ab68352], 1:200) at 4°C overnight. The membranes were then washed 4× with TTBS (10 min each) and incubated with secondary antibody (mouse [ab97046], rabbit [sc-2004], 1:2,000) at RT for 1 h. The membranes were finally washed 4× with TTBS (10 min each). To correct for loading error and to normalize the expression of the proteins, β-actin was assessed (ab8226; 1:2,000). Horseradish peroxidase chemiluminescence detector and enhancer solution was used for the antigen-antibody complex and the signal was detected with the Alliance 2.7 image documentation system (UViTech). The expression of the proteins was analyzed with UViBand Advanced Image Analysis software (UViTech, v12.14). The data was expressed as relative band density (RBD) and fold change.

QUANTIFICATION OF mRNA

To determine *c-myc*, *p53*, *skp2*, and *Fbw7α* mRNA levels in A549 cells, RNA was first isolated from the control and ML_{AuNP} treatment by adding 500 µl Tri reagent (Life technologies Am9738) as per manufacturer's guidelines. Thereafter, RNA was quantified (Nano-drop 2000) and standardized to 600 ng/µl. RNA was reverse transcribed by reverse transcriptase into copy DNA (cDNA) using the iScript™ cDNA synthesis kit (Bio-Rad, SA, cat. no. 1708891) as per manufacturer's instructions. Briefly, a 20 µl reaction was prepared by adding 4 µl 5× iScript reaction mix, 1 µl iScript reverse transcriptase, 12 µl nuclease free water, 3 µl RNA template. The reaction was then subjected to 25°C (5 min), 42°C (30 min), 85°C (5 min), and a final hold at 4°C (CFX96 Real Time thermal cycler [Bio-Rad, SA]) to obtain cDNA.

Quantitative PCR (qPCR) was used to determine mRNA levels using iQ Superscript reagent (Bio-Rad, SA). A 25 µl reaction consisting of 12.5 µl IQ™ SYBR® green supermix (Bio-Rad, SA, cat. no. 170–8880), 8.5 µl nuclease free water, 2 µl cDNA, and 1 µl sense and anti-sense primer (10 mM, Inqaba Biotec, SA, Table I) were used. The mRNA levels was compared and normalized to a housekeeping gene, *GAPDH*. The reaction was subjected to an initial denaturation (95°C, 8 min). It was followed by 40 cycles of denaturation (95°C, 15 s), annealing (*c-myc*, *p53*, *Skp2*, *Fbw7α*: 56°C, 40 s) and extension (72°C, 30 s) (CFX96 Real Time thermal cycler [Bio-Rad, SA]). The data was analyzed using CFX Manager™ software V3.0 (Bio-Rad, SA). The mRNA levels was determined using the Livak method and expressed as fold changes [Livak and Schmittgen, 2001].

ALTERNATE SPLICING OF *CASPASE-9*

To determine the expression of *caspase-9* splice variants, *caspase-9* sense primer (5′-GCTCTTCCTTTGTTCATCTCC-3′) and anti-sense primer (5′-CATCTGGCTCGGGGTTACTGC-3′) (10 mM, Inqaba Biotec) were used [Massiello and Chalfant, 2006; Shultz et al., 2010; Shultz et al., 2011]. The reaction was subjected to an initial denaturation (94°C, 8 min). It was followed by 35 cycles (20% of the reverse transcriptase reaction was amplified) of denaturation (94°C, 30 s), annealing (*caspase-9*: 58°C, 30 s), and extension (72°C, 1 min) (CFX96 Real Time thermal cycler [Bio-Rad, SA]). The qPCR product was examined on 1.5% agarose gel using Alliance 2.7 image documentation system (UViTech). Densitometric analysis (UViBand Advanced Image Analysis software [UViTech, v12.14]) was conducted to assess *caspase-9a* and *caspase-9b* splice variant. The data was expressed as RBD and ratio of *caspase-9a*/*caspase-9b*.

STATISTICAL ANALYSIS

Statistical analyses were performed using GraphPad Prism v5.0 software (GraphPad Software Inc., La Jolla). The results were expressed as means with standard error of the mean (SEM). The comparisons and statistical significance were determined by unpaired *t*-test and a 95% confidence interval. The data were considered statistically significant with a value of $P < 0.05$.

RESULTS

PHYTOCHEMICAL ANALYSIS OF *MORINGA* OLEIFERA AQUEOUS LEAF EXTRACT

Moringa oleifera aqueous leaf extract showed eleven peaks in the GC-MS chromatogram (Fig. 1). The compounds were separated according to their retention time on fused silica capillary column.

TABLE I. Primer Sequences Used in qPCR Assay

	Primer sequences	
	Sense primer	Anti-sense primer
c-myc	5′-AGCGACTCTGAGGAGGAACAAG-3′	5′-GTGGCACCTCTTGAGGACCA-3′
p53	5′-CCACCATCCACTACAACTACAT-3′	5′-CAAACACGGACAGGACCC-3′
Skp2	5′-TGGGAATCTTTTCCTGTCTG-3′	5′-GAACACTGAGACAGTATGCC-3′
Fbw7α	5′-AGTAGTATTGTGGACCTGCCCGTT-3′	5′-GACCTCAGAACCATGGTCCAACTT-3′
GAPDH	5′-TCCACCACCCTGTTGCTGTA-3′	5′-ACCACAGTCCATGCCATCAC-3′

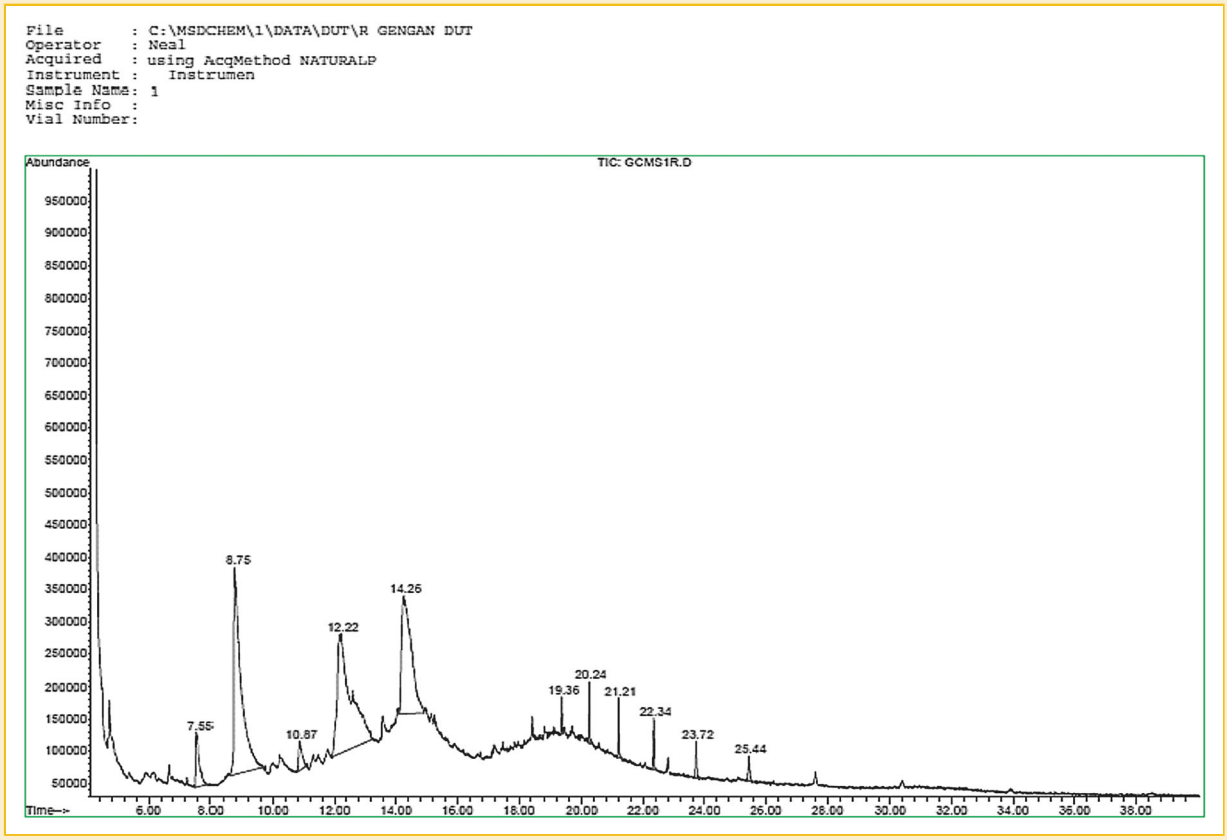

Fig. 1. Chemical composition of *Moringa oleifera* aqueous leaf extract by GC–MS analysis.

The total ion chromatogram (TIC) indicates the presence of various organic compounds with significant abundant peaks at retention time 7.55, 8.75, 10.87, 12.22, 14.26, 19.36, 20.24, 21.21, 22.34, 23.72, and 25.44 min having molecular ions (*m/z*) of 144.0, 126.0, 142.0, 58.0, 60.0, 310.0, 338.0, 352.0, 279.0, 366.0, and 380.0, respectively. These compounds mainly comprised of hydrocarbons and phenolic compounds. Pyran-4-one (7.55), 2-Furancarboxaldehyde (8.75), Docosane (19.36), Tetracosane (21.21), Pentacosane (22.34), Heptacosane (23.72) identified as major chemical constituents followed by Octacosane (25.44) [Al-Owaisi et al., 2014].

SYNTHESIS OF ML_{AuNP}

The molar calculation of the crude leaf extract cannot be determined. We synthesized the ML_{AuNP}′s on the basis of weight percent ratios of leaf extract and gold chloride. In the present study—5 g of leaf in 100 ml water and 0.0393 g of gold chloride in 100 ml of water, making the final W% ratio is 5:0.039% [Shankar et al., 2004].

A color change to red-brown (Fig. 2.1) within a few seconds of mixing the leaf extract with the $HAuCl_4$ solution supported the formation of ML_{AuNP}′s. This was attributed to the excitation of surface plasmon vibrations in gold nanoparticles. The observation validated the reduction of Au^{3+} ions to Au by the plant components. The Surface Plasmon Resonance (SPR) is visible as a broad band at λ_{max} 542 nm (Fig. 2.1), consistent with literature [Stuchinskaya et al., 2011]. The UV-visible absorption spectra of both aqueous leaf extract (Fig. 2.2A) as well as gold chloride solution (Fig. 2.2B) is shown.

The obtained ML_{AuNP}′s dispersion was stable for over 6 months at room temperature. The peak at 544 nm in UV-visible absorption spectra (Fig. 2.3) is attributed to the SPR of stable AuNPs. Also, the plasmon band has been sharp and symmetric, which indicates that the solution does not contain much of aggregated particles after 6 months.

The transmission electron microscopy (TEM) micrographs and size distribution of the ML_{AuNP}′s indicated that most of the particles are spherical or near spherically shaped, however, some polyhedral particles are also present. It was also observed that the ML_{AuNP}′s were highly poly-dispersed in the colloidal solution. ML_{AuNP}′s had a large size distribution (10–20 nm) (Fig. 3).

The size distribution of ML_{AuNP} was determined by DLS. The average hydrodynamic size was 26.44 nm (Figs. 4 and 5) which were similar to *Melia azedarach′s* leaf extract [Sukirtha et al., 2012]. The ML_{AuNP} size obtained from TEM and DLS was different. This can be attributed to the different principles applied for determining the size distribution.

Many reports have proposed that surface active molecules can stabilize the nanoparticles and that the reaction of the metal ions is possibly facilitated by reducing sugars and or plant based organic molecules. However, a stable dispersion of particles was evident from the zeta potential of −25.3 mV (Fig. 6); a zeta potential higher than

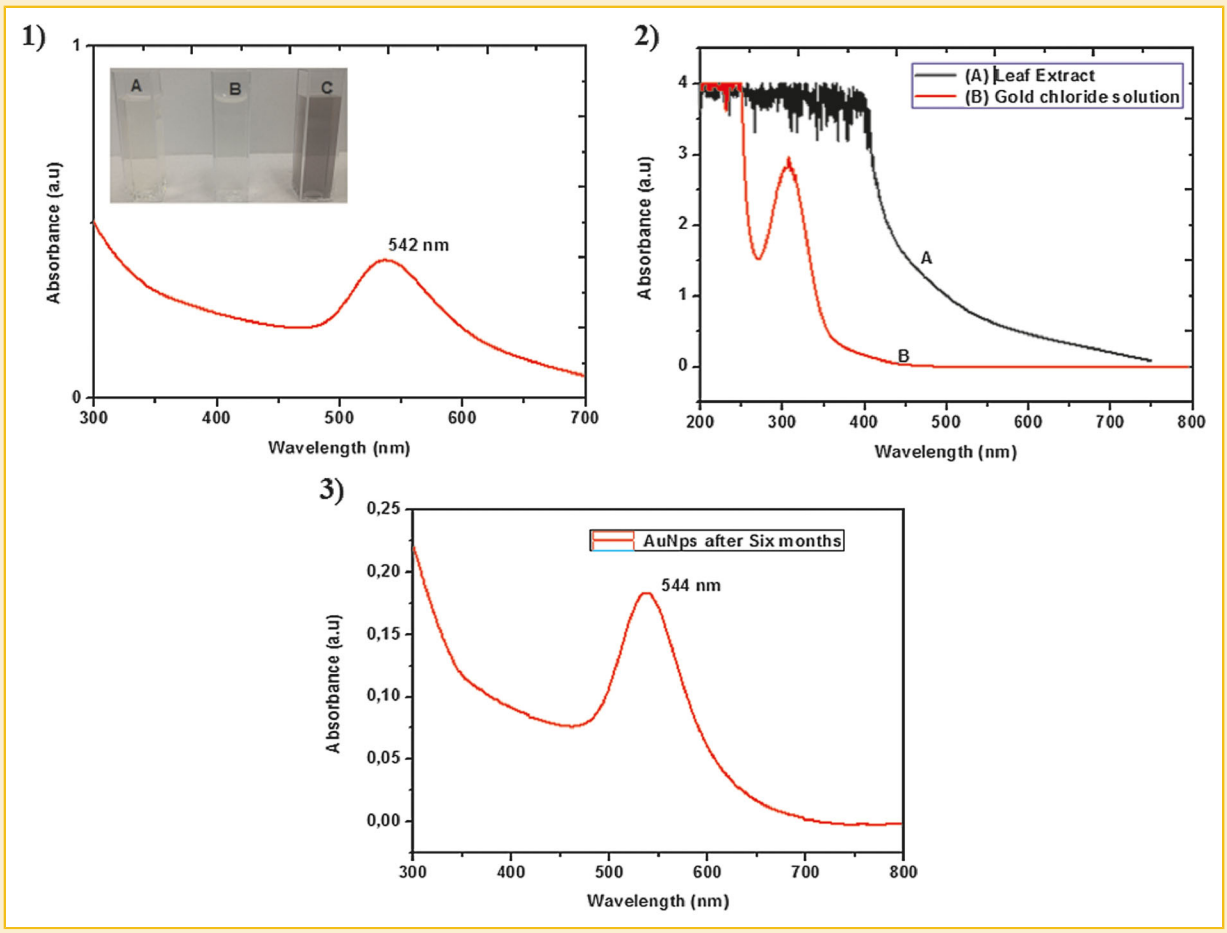

Fig. 2. The UV-visible absorption spectra of (1) AuNP's biosynthesized by aqueous leaf extract of *Moringa oleifera* insert 2.1: The color change when ML_{AuNP}'s were formed (A) Aqueous leaf extract (B) Gold chloride solution (C) Gold nanoparticles. (2) (A) Aqueous leaf extract (B) Gold chloride solution. (3) Stability of ML_{AuNP}'s at 544 nm UV-visible absorption spectra analysis after 6 months.

30 mV or lesser than −30 mV is indicative of a stable system [Kotakadi et al., 2014].

CELL VIABILITY ASSAY

ML_{AuNP} and trisodium citrate AuNPs (C_{AuNP}) (synthesized by conventional chemical methods) cytotoxicity in A549 lung cancer cells, SNO oesophageal cancer cells and normal healthy PBMCs was then determined using the MTT assay. C_{AuNP} and ML_{AuNP} treatment for 24 h caused a dose-dependent decline in A549 and SNO cell viability. C_{AuNP} IC_{50} value was determined as 121.4 μg/ml (A549) and 410.4 μg/ml (SNO) (Fig. 7A). An IC_{50} value of 98.46 μg/ml (A549) and 92.01 μg/ml (SNO) was calculated for ML_{AuNP} (Fig. 7B). Furthermore, C_{AuNP} and ML_{AuNP} showed no cytotoxicity in normal healthy PBMCs (Fig. 7A and B, respectively) and an IC_{50} value was unable to be determined.

ASSESSMENT OF APOPTOSIS INDUCTION

The percentage of apoptosis induced in both A549 and SNO cells by ML_{AuNP} is presented in Tables II and III.

An early marker of apoptosis is PS externalization which was significantly increased in A549 cells (3.88-fold, Table III). ML_{AuNP} altered mitochondrial function by significantly increasing $\Delta\Psi m$ (1.43-fold) and simultaneously decreasing ATP levels (1.20-fold) (Tables II and III) in A549 cells. The ATP levels in SNO cells were decreased by C_{AuNP} and ML_{AuNP} (1.01-fold and 5.05-fold, respectively) (Table II). Also, executioner caspase-3/7 (1.34-fold) and initiator caspase-9 (1.14-fold) activities were increased by ML_{AuNP} treatment in A549 cells as compared to the control (Table II). In addition, C_{AuNP} and ML_{AuNP} increased executioner caspase-3/7 significantly in SNO cells (2-fold and 2.5-fold, respectively) (Table II). Also initiator caspase-9 increased after exposure to C_{AuNP} and ML_{AuNP} in the cancerous SNO cells (1.01-fold and 1.12-fold, respectively) (Table II).

WESTERN BLOTTING

The relative protein levels of c-myc, p53, SRp30a, Bax, Bcl-2, Smac/DIABLO, Hsp70, and PARP-1 were assessed using Western blot (Fig. 8).

Oncogenes such as c-myc are responsible for cell proliferation and tumor progression [Bonomi et al., 2013]. In A549 lung cancer cells, exposure to ML_{AuNP} caused a significant 1.56-fold decrease in c-myc levels (0.04 ± 0.00 RBD vs. control: 0.07 ± 0.00 RBD, $P < 0.05$)

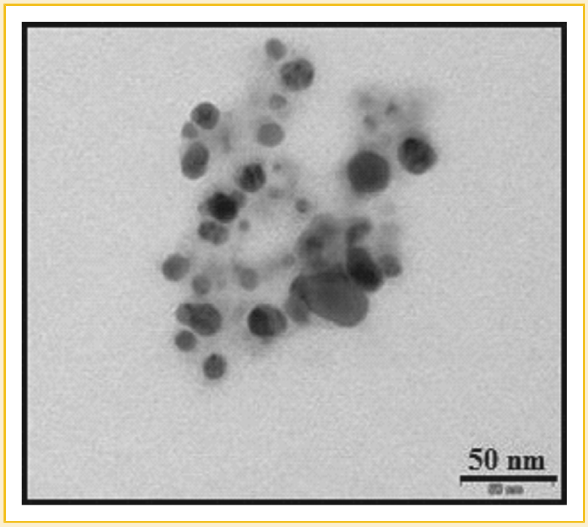

Fig. 3. Representative TEM micrograph of ML_{AuNP}'s biosynthesized by aqueous leaf extract of *Moringa oleifera*. The ML_{AuNP} shape was determined to be spherical or near spherical and polyhedral with size of 10–20 nm.

(Fig. 8). This led to the assessment of p53, a tumor suppressor gene which was significantly increased by 1.17-fold (0.13 ± 0.00 RBD vs. control: 0.11 ± 0.01, $P < 0.05$) (Fig. 8). ML_{AuNP} treated A549 cells further demonstrated a significant increase in pro-apoptotic proteins such as Bax (1.34-fold, 0.12 ± 0.00 RBD vs. control: 0.09 ± 0.00 RBD, $P < 0.001$) and Smac/DIABLO levels (1.52-fold, 0.10 ± 0.00 RBD vs. control: 0.07 ± 0.00 RBD, $P < 0.0001$) (Fig. 8).

During apoptosis PARP-1 is cleaved and exposure to ML_{AuNP} caused the cleavage and activation of PARP-1. A 1.30-fold increase in PARP-1 24 kDa fragment was seen (0.23 ± 0.00 RBD vs. control: 0.17 ± 0.00 RBD, $P < 0.0001$) (Fig. 8). Interestingly, SRp30a, an alternate splicing factor, was increased by 1.13-fold in A549 treated cells (0.05 ± 0.01 RBD vs. control: 0.04 ± 0.00 RBD, $P = 0.428$) (Fig. 8). In addition, anti-apoptotic Bcl-2 protein was decreased (1.30-fold) by ML_{AuNP} compared to the control (0.11 ± 0.01 RBD vs. 0.14 ± 0.01 RBD, $P < 0.05$) (Fig. 8). Furthermore, Hsp70 was also significantly reduced (1.30-fold, 0.57 ± 0.00 RBD vs. control: 0.73 ± 0.02 RBD, $P < 0.0001$) (Fig. 8).

QUANTIFICATION OF mRNA

The mRNA levels of *c-myc*, *p53*, *skp2*, and *Fbw7*α in A549 cells was determined using qPCR relative to the control (Fig. 9). The *c-myc* mRNA levels were decreased 1.44 ± 0.05-fold ($P < 0.001$) in ML_{AuNP} treatment (Fig. 9). A 1.77 ± 0.12-fold ($P < 0.05$) increase in *p53* mRNA levels was observed in ML_{AuNP} treated cells. *Skp2* levels decreased by 7.33-fold ± 0.01 ($P < 0.0001$) and *Fbw7*α decreased by 2.82-fold ± 0.04 ($P < 0.0001$) in ML_{AuNP} treatment (Fig. 9).

ALTERNATE SPLICING OF *CASPASE-9*

Alternate splicing pattern of *caspase-9* was determined using qPCR and presented in Figure 10.

ML_{AuNP} activated alternate splicing of *caspase-9* in A549 cancer cells resulting in both a significant 1.68-fold ($P < 0.001$) increase in pro-apoptotic *caspase-9a* and a 1.67-fold ($P < 0.05$) decrease in *caspase-9b* levels (Fig. 10). Analysis of the alternate splice variants of *caspase-9* showed that ML_{AuNP} changed the *caspase-9a/caspase-9b* ratio from 0.63 ± 0.03 to 1.76 ± 0.08 in the cancer cells.

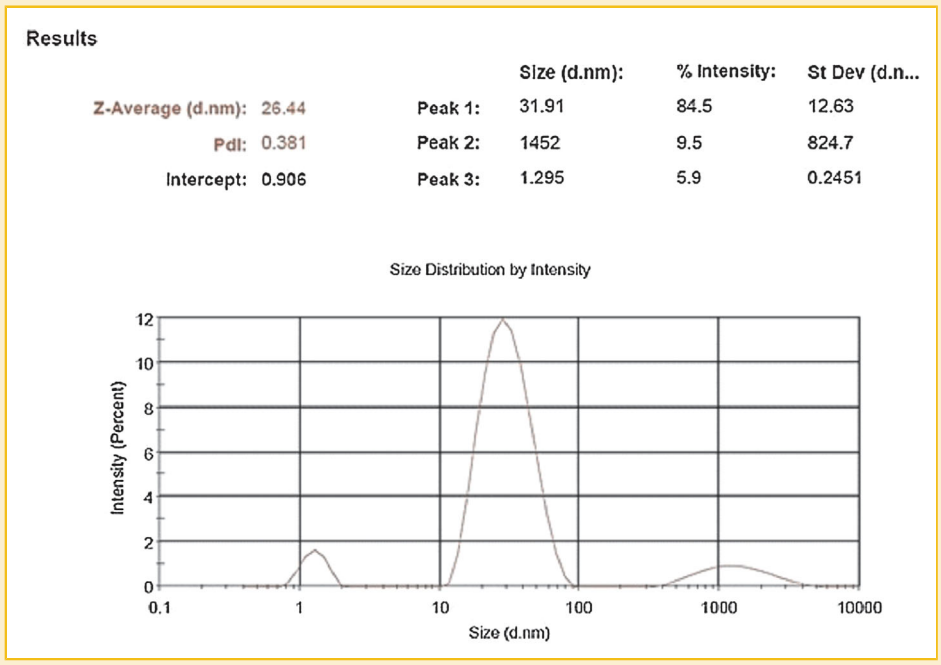

Fig. 4. The hydrodynamic size of ML_{AuNP} showed a maximum intensity at 26.44 nm as determined by DLS.

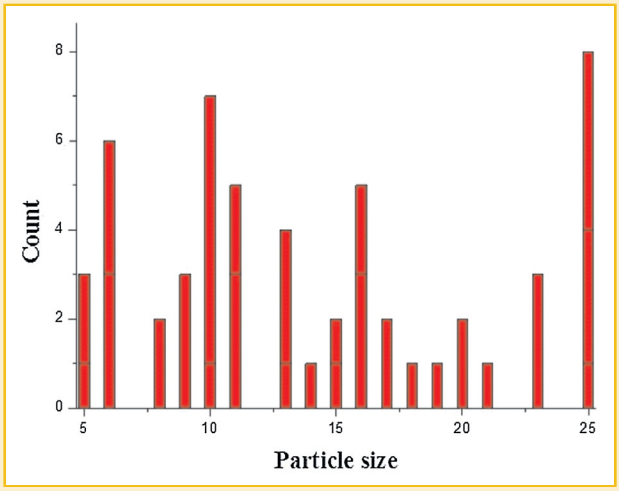

Fig. 5. The size distribution of ML_{AuNP} (Image J).

DISCUSSION

Lung cancer is characterized by uncontrolled cell growth, loss of normal functionality and evasion of apoptosis [Ho et al., 2010]. Current anticancer therapies possess adverse effects and are becoming drug resistant and hence new and more effective agents are actively being investigated. An effective treatment regime for lung cancer will not only increase survival rates but also improve quality of life [Montazeri et al., 2001]. Nanoparticles have huge potential in the treatment of various cancers [Lim et al., 2011; Selim and Hendi, 2012]. ML_{AuNP} was synthesized using MO crude aqueous leaf extract in an environmentally friendly synthesis (Figs. 2–6). The leaf components possess reducing potential which aided in the green synthesis of the AuNP′s [Anand et al., 2014]. There are many phytochemicals present in the leaf extract which includes phenolic acids and flavonoids such as gallic acid, itaconic acid, and catechol [Luqman et al., 2012; Belliraj et al., 2015; El Sohaimy et al., 2015]. In addition, the chemical composition of *Moringa oleifera* aqueous leaf extract by GC-MS analysis showed that it mainly contained hydrocarbons and phenolic compounds (Fig. 1). Pyran-4-one, 2-Furancarboxaldehyde, Docosane, Tetracosane, Pentacosane, Heptacosane, and Octacosane were identified as major chemical constituents. They play a role in the reduction of the metal ions to form the gold nanoparticles. Gallic acid, a bioactive compound present in the leaf extract can act as a reducing and stabilizing agent [Li et al., 2015]. ML_{AuNP} and C_{AuNP} induced cytotoxicity and decreased cell viability in A549 lung and SNO oesophageal cancer cells in a dose-dependent manner (Fig. 7), whilst no cytotoxicity was observed in normal healthy PBMCs (Fig. 7). ML_{AuNP} as compared to C_{AuNP}, induced greater cytotoxicity and increased antiproliferative effects in both cancerous A549 and SNO cells, reducing A549 and SNO cell viability to 19% and 31%, respectively. However C_{AuNP} only reduced A549 and SNO cell viability to 53% and 44%, respectively. This shows the selective targeting of AuNP′s to cancerous cells, with increased selectivity by the ML_{AuNP}. In addition, ML_{AuNP} was not cytotoxic to normal healthy PBMC′s and the increased PBMC′s cell viability may be due to the bioactive compounds present in the aqueous crude leaf extract such as glutamine [Roth et al., 2002; Ndubuaku et al., 2013]. Due to minimal toxicity observed in PBMCs, we investigated the mechanism of cell death induced by ML_{AuNP} in A549 and SNO cells.

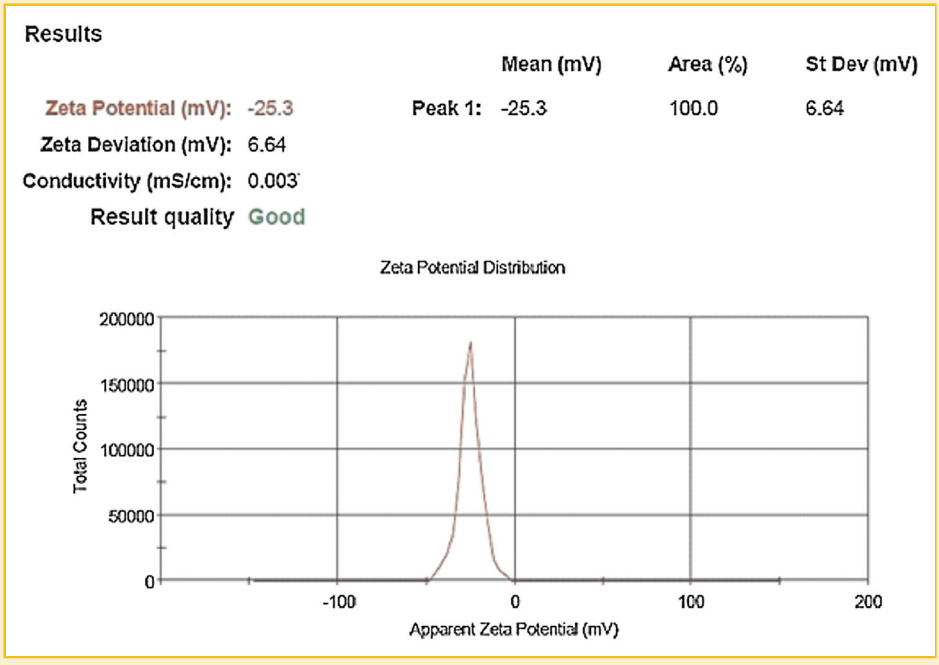

Fig. 6. Stability of ML_{AuNP}'s at −25.3 mV in zeta potential analysis.

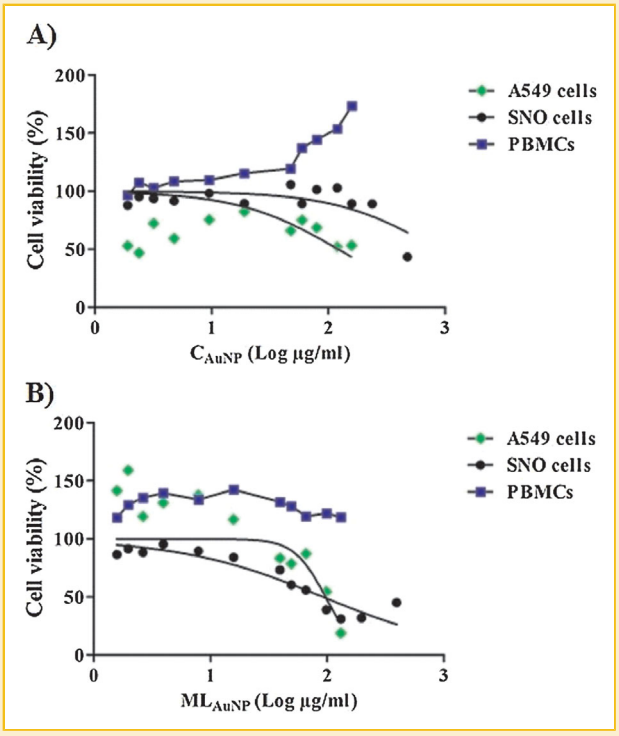

Fig. 7. Percentage A549, SNO, and PBMCs cell viability after exposure to C_{AuNP} and ML_{AuNP} for 24 h. The MTT assay was used to determine A549, SNO, and PBMCs cell viability. A dose-dependent decline in A549 and SNO cell viability was observed whereas no cytotoxicity was observed in PBMCs.

TABLE III. Phosphatidylserine Externalization and Mitochondrial Depolarization in A549 Cells Following Treatment With ML_{AuNP} for 24 h

	A549 cells (mean ± SEM)	
	Control	ML_{AuNP}
PS extenalization (%)	1.03 ± 0.07	3.99 ± 0.04***
ΔΨm (%)	16.70 ± 0.50	23.90 ± 0.20**,[a]

SEM, standard error of the mean; PS, Phosphatidylserine; ΔΨm, Mitochondrial depolarization.
[a]Significantly different compared to control.
**$P < 0.001$.
***$P < 0.0001$.

The c-myc oncoprotein, a basic helix-loop-helix leucine-zipper transcription factor, regulates genes controlling cell growth and proliferation [An et al., 2008]. Lung cancer cells have increased c-myc expression. The ubiquitin-proteasome pathway is responsible for the proteolysis of c-myc involving the F-box protein and ubiquitin ligase components, while *c-myc* mRNA and protein stability contributes to its role in carcinogenesis [Kim et al., 2014]. Posttranslational regulation of c-myc is via Skp2 and Fbw7α [Chen et al., 2013], that are different regulation subunits of the SCF-type E3 ligase (Skp1/Cullin/F-box protein complexes) responsible for proteasomal degradation. The c-myc/Skp2/Fbw7α pathway is linked to tumor progression and is therefore a potential target for anticancer agents [Chen et al., 2013]. c-Myc increases Skp2 expression which also acts as a co-factor increasing c-myc's transcriptional activity [Kim et al., 2014]. Glycogen synthase kinase 3 (Gsk3) mediates Fbw7α degradation of c-myc. Gsk3 phosphorylates threonine 58 residue on c-myc which serves as a recognition site for Fbw7α. ML_{AuNP} significantly decreased both *c-myc* mRNA and protein expression in A549 cells (Figs. 8 and 9). Also Skp2 levels were significantly decreased (Fig. 9). This influences c-myc's transcriptional function hence the inhibition of its proliferative effect. In addition, Skp2 causes the degradation of p27 (cyclin dependent kinase inhibitor) thus allowing cell proliferation and therefore loss of Skp2 function will result in p27 induced cell cycle arrest and inhibition of cell proliferation [Dai et al., 2006; Kim et al., 2014]. Drug resistant cancers often have decreased Fbw7 expression which acts as a tumor suppressor [Dai et al., 2006; Chen et al., 2013]. ML_{AuNP} significantly decreased *Fbw7*α mRNA levels (Fig. 9). The anticancer effect of Wogonin in A549 cells was due to decreased c-myc, Skp2, and Fbw7α levels [Chen et al., 2013]. The induction of apoptosis occurred independently of Fbw7α. Similarly, ML_{AuNP} decreased c-myc, Skp2, and Fbw7α levels suggesting a possible role in drug-resistant cancers.

The p53 tumor suppressor gene functions by regulating cell growth, proliferation and apoptosis. In cancer cells, p53 function is often dysregulated thereby allowing abnormal cells to continue to proliferate. ML_{AuNP} treatment caused a significant increase in *p53* mRNA and protein expression (Figs. 8 and 9). A consequence of increased p53 expression resulted in increased expression of Bax, a pro-apoptotic protein and a simultaneous decrease in the anti-apoptotic Bcl-2 protein (Fig. 8). Furthermore the induction of

TABLE II. ATP and Caspase Activity in A549 and SNO Cells Following Treatment With ML_{AuNP} for 24 h

	A549 cells (mean ± SEM)		SNO cells (mean ± SEM)		
	Control	ML_{AuNP}	Control	C_{AuNP}	ML_{AuNP}
ATP (×10^5 RLU)	20.47 ± 0.13	17.12 ± 0.33***	33.36 ± 0.44	32.96 ± 0.86	6.61 ± 0.05***
Caspase-3/7 (×10^5 RLU)	0.54 ± 0.02	0.73 ± 0.03**	0.02 ± 0.00	0.04 ± 0.00[a]	0.05 ± 0.00**
Caspase-9 (×10^5 RLU)	4.34 ± 0.00	4.94 ± 0.09*	1.96 ± 0.00	1.97 ± 0.04	2.20 ± 0.00*

SEM, standard error of the mean; RLU, relative light unit.
[a]Significantly different compared to control.
*$P < 0.05$.
**$P < 0.001$.
***$P < 0.0001$.

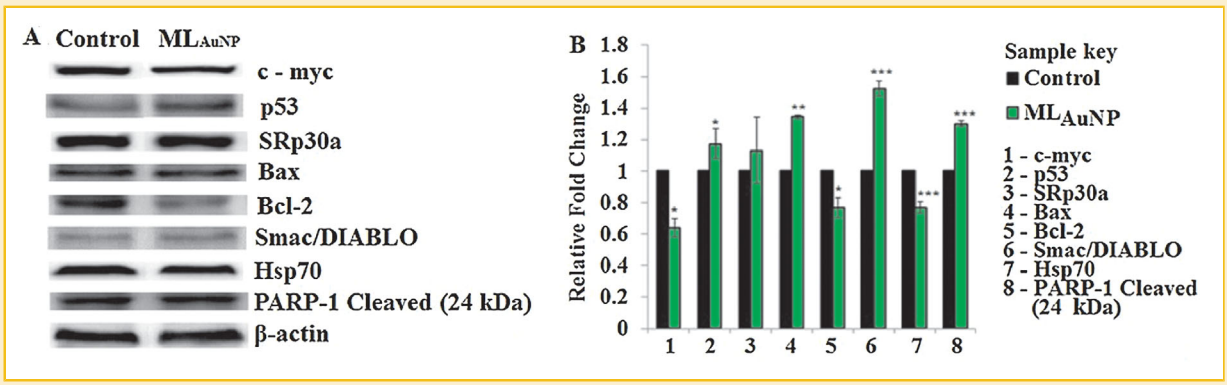

Fig. 8. The effect of ML_{AuNP} on protein levels in A549 cells. Western blot analysis of protein levels (A) and the relative fold change (B) in A549 lung cancer cells after exposure to ML_{AuNP} ($^{***}P < 0.0001$, $^{**}P < 0.001$, and $^{*}P < 0.05$). Apoptotic proteins were significantly increased with a simultaneous decrease in anti-apoptotic proteins. Protein bands were normalized against β-actin.

apoptosis through the activation of Bax causes it to bind to voltage-dependent anion channel (VDAC) and influences its activity [Hengartner, 2000]. The VDAC protein forms a subunit of the mitochondrial permeability transition pore (MPTP). The depolarization of the mitochondrial membrane by ML_{AuNP} opens the MPTP resulting in cytochrome c (cyt c) release from the mitochondria into the cytoplasm, together with ATP. A consequence is that Apaf-1 cleaves procaspase-9 resulting in activation of caspase-9 (Table II).

The regulation of gene and protein expression is a determinant of cell fate. The serine/arginine-rich proteins (SR proteins) are required for alternate splicing [Manley and Krainer, 2010]. The alternate pre-mRNA processing of *caspase-9* gene produces two splice variants, the pro-apoptotic *caspase-9a*, and the anti-apoptotic *caspase-9b* [Massiello and Chalfant, 2006; Shultz et al., 2010; Shultz et al., 2011]. The inclusion of exon 3, 4, 5, and 6 cassette results in *caspase-9a* splice variant and the induction of apoptosis. *Caspase-9b* (exon exclusion) competes with *caspase-9a* for binding to the apoptosome.

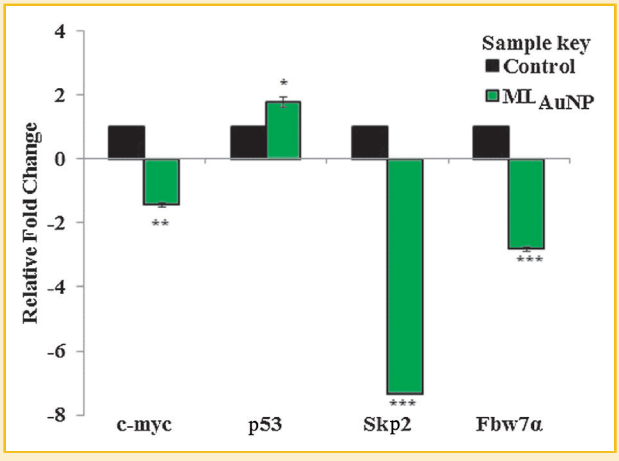

Fig. 9. The mRNA levels of c-myc, p53, skp2, and Fbw7α in A549 cells. mRNA levels were differential expressed in A549 cells after exposure to ML_{AuNP} for 24 h ($^{***}P < 0.0001$, $^{**}P < 0.001$, and $^{*}P < 0.05$).

SRp30a is an important splicing factor in the alternative splicing of *caspase-9* [Massiello and Chalfant, 2006] and ML_{AuNP} increased SRp30a protein expression (Fig. 8) thus activating alternate splicing of pre-mRNA in A549 cells. There was a significant increase in *caspase-9a* with a concomitant decrease in *caspase-9b* mRNA levels in A549 cells (Fig. 10). ML_{AuNP} increased the *caspase-9a/caspase-9b* ratio from 0.63 to 1.76. Our findings are consistent with those of Massiello and Chalfant [2006], where ceramide treated A549 cells resulted in alternate splicing of *caspase-9* with increased *capase-9a* and decreased *caspase-9b* splice variants [Massiello and Chalfant, 2006]. The ratio of *caspase-9a/caspase-9b* increased after ceramide treatment. Also SRp30a was identified as the RNA *trans*-acting factor (regulating splicing factor) involved in the pre-mRNA processing and its downregulation favoured *caspase-9b* at the expense of *caspase-9a* [Massiello and Chalfant, 2006]. The increased expression of *caspase-9a* splice variant by ML_{AuNP} resulted in an increase in caspase-9 activity. Increased caspase-9 caused activation of the executioner caspases-3/7 leading to apoptosis (Table II). These observations strongly suggest that ML_{AuNP} preferentially targets the mitochondria and induces apoptosis via the intrinsic pathway. Furthermore, ML_{AuNP} in SNO cells displayed a greater increase in caspase activity as compared to C_{AuNP} (Table II). The results show that ML_{AuNP} can be used as an antiproliferative agent.

In addition, during the execution of apoptosis, poly (ADP-ribose) polymerase 1 (PARP-1), a nuclear enzyme, is cleaved into an 89 kDa C-terminal catalytic fragment and a 24 kDa N-terminal DNA-binding domain fragment [D'Amours et al., 2001]. ML_{AuNP} actively induced PARP-1 cleavage in A549 cells as evidenced by the significant increase in the 24 kDa fragment (Fig. 8) confirming the execution of apoptosis. Further, PS externalization [Schlegel and Williamson, 2001] was also significantly increased by ML_{AuNP} (Table II).

Inhibitor of apoptosis protein (IAP), contain baculoviral IAP repeat (BIR) domains, is an intracellular protein that inhibits caspase activity [Hengartner, 2000; Wang, 2001]. Smac/DIABLO which is concurrently released with cyt c from the mitochondria, binds to the BIR domain of IAP thus antagonising its action and ensures the execution of apoptosis [Fischer and Schulze-Osthoff, 2005]. ML_{AuNP}

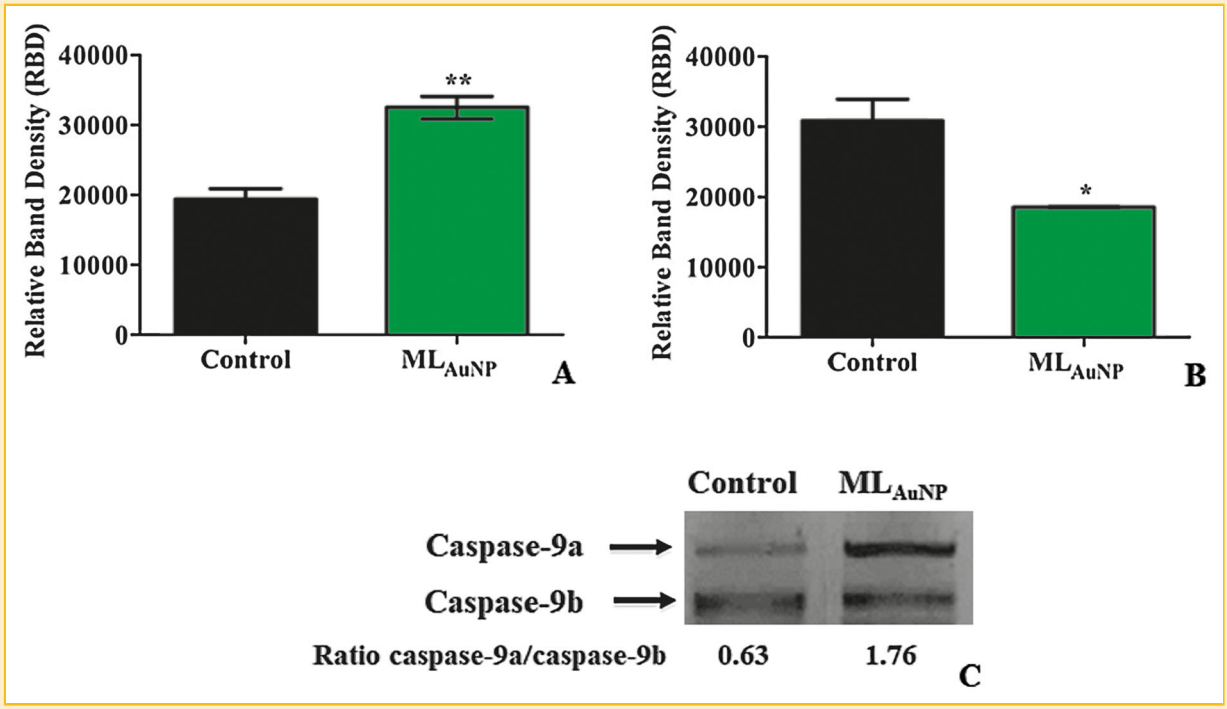

Fig. 10. The effect of ML_{AuNP} on alternate splicing of *caspase-9* in A549 cells. *Caspase-9a* (A) and *caspase-9b* (B) levels were determined by densitometric analysis of qPCR product (C) ($^{**}P < 0.001$, $^{*}P < 0.05$). ML_{AuNP} activated alternate splicing with a significant increase in caspase-9a splice variant.

significantly increased Smac/DIABLO protein levels (Fig. 8). Our data clearly shows that ML_{AuNP} induces and promotes apoptosis in A549 lung cancer cells. Hsp70, a chaperone molecule, inhibits key effectors in apoptosis [Garrido et al., 2006] and are highly expressed in cancer cells. Hsp70 inhibits apoptosome formation as it binds to Apaf-1 and prevents the recruitment of procaspase-9, thus inhibiting apoptosis and enabling the cancer cells to continue proliferation. In our study, Hsp70 expression was significantly reduced by ML_{AuNP} (Fig. 8), thus ensuring the effective execution of apoptosis and the inability of the cancer cells to continue proliferation.

Selim and Hendi, [2012] showed the induction of apoptosis by chemically synthesized AuNP′s in an MCF-7 (breast cancer) cell line [Selim and Hendi, 2012]. AuNP′s significantly increased p53, Bax, caspase-3 and caspase-9, and decreased Bcl-2 expression. Another study showed that AuNP′s decreased GSH levels, increased mitochondrial depolarization and ultimately led to cell death in HL7702 cells [Gao et al., 2011]. Chemically synthesized AuNP′s also caused A549 cell cycle arrest and accumulation in the G1 phase of the cell cycle [Chuang et al., 2013]. Green synthesis of AuNP′s using a plant extract from *Podophyllum hexandrum* showed antiproliferative properties in human cervical carcinoma cells (HeLa cells) [Jeyaraj et al., 2014]. The green synthesis of AuNP′s by MO leaves shows promise as an anticancer agent by inducing increased apoptosis in lung cancer cells. The development of nanoparticles has shown potential in therapies which ultimately improve survival rates [Leong and Ng, 2014]. Synthesized AuNP′s inhibited ovarian cancer cell growth in a size and concentration dependent manner [Arvizo et al., 2013]. It also inhibited MAPK-signalling with a reversal of the epithelial-mesenchymal transition in the cancer cells displaying antiproliferative and anti-metastatic properties. The physico-chemical properties of NP′s depends on the size, shape, charge, hydrophobicity as well as functional groups which facilitates their interaction with biological systems however the mechanism of action is still to be fully elucidated [Davis et al., 2008; Tay et al., 2014].

ML_{AuNP} was successfully produced in a one-pot green synthesis by MO leaves. The synthesized ML_{AuNP} was not cytotoxic to normal healthy PBMCs but was cytotoxic and induced apoptosis, via the intrinsic pathway, in cancerous A549 lung cells. ML_{AuNP} targeted oncogenes, tumor suppressor genes and was able to activate alternate splicing of *caspase-9* to effectively execute the apoptotic cascade in lung cancer cells. In addition, ML_{AuNP} caused a dose-dependent decrease in SNO cancer cell viability and activated caspase activity, showing that ML_{AuNP} has an affinity affect cancer cells. Further, ML_{AuNP} showed greater reduction in cell viability in A549 cells as compared to Trisodium citrate gold nanoparticles (C_{AuNP}) (chemically synthesized gold nanoparticles); ML_{AuNP} as compared to C_{AuNP} also induced higher caspase activity in cancerous SNO cells—showing it specifically targets cancer cells.

ACKNOWLEDGMENTS

Miss C. Tiloke acknowledges the prestigious Doctoral scholarship from the National Research Foundation, SA. The study was also supported by the funds from College of Health Sciences (UKZN).

REFERENCES

Al-Owaisi M, Al-Hadiwi N, Khan SA. 2014. GC-MS analysis, determination of total phenolics, flavonoid content and free radical scavenging activities of various crude extracts of *Moringa peregrina* (Forssk.) Fiori leaves. Asian Pac J Trop Biomed 4:964–970.

An J, Yang D, Xu Q, Zhang S, Huo Y, Shang Z, Wang Y, Wu D, Zhou P. 2008. DNA-dependent protein kinase catalytic subunit modulates the stability of c-Myc oncoprotein. BMC Mol Cancer 7:1–12.

Anand K, Gengan R, Phulukdaree A, Chutugoon AA. 2014. Agroforestry waste *Moringa oliefera* petals mediated green synthesis of gold nanoparticles and their anti-cancer and catalytic activity. J Ind Eng Chem 21:1105–1111.

Arvizo RR, Saha S, Wang E, Robertson JD, Bhattacharya R, Mukherjee P. 2013. Inhibition of tumor growth and metastasis by a self-therapeutic nanoparticle. Proc Natl Acad Sci 110:6700–6705.

Bainor A, Chang L, McQuade TJ, Webb B, Gestwicki JE. 2011. Bicinchoninic acid (BCA) assay in low volume. Anal Biochem 410:310–312.

Belliraj TS, Nanda A, Ragunathan R. 2015. In-vitro hepatoprotective activity of *Moringa oleifera* mediated synthesis of gold nanoparticles. J Chem Pharm Res 7:781–788.

Bello B, Fadahun O, Kielkowski D, Nelson G. 2011. Trends in lung cancer mortality in South Africa: 1995–2006. BMC Public Health 11:2–5.

Bonomi S, Gallo S, Catillo M, Pignataro D, Biamonti G, Ghigna C. 2013. Oncogenic alternative splicing switches: Role in cancer progression and prospects for therapy. Int J Cell Biol 1–17.

Cai W, Gao T, Hong H, Sun J. 2008. Applications of gold nanoparticles in cancer nanotechnology. Nanotechnol Sci Appl 1:17–32.

Chen X, Bai Y, Zhong Y, Xie X, Long H, Yang Y, Wu S, Jia Q, Wang X. 2013. Wogonin has multiple anti-cancer effects by regulating c-Myc/Skp2/Fbw7α and HDAC1/HDAC2 pathways and inducing apoptosis in human lung adenocarcinoma cell line A549. PLoS ONE 8:1–7.

Cheng Y, Lee S, Lin S, Chang W, Chen Y, Tsai N, Liu Y, Tzao C, Yu D, Harn H. 2005. Anti-proliferative activity of *Bupleurum scrozonerifolium* in A549 human lung cancer cells in vitro and in vivo. Cancer lett 222:183–193.

Chuang S, Lee Y, Liang R, Roam G, Zeng Z, Tu H, Wang S, Chueh PJ. 2013. Extensive evaluations of the cytotoxic effects of gold nanoparticles. Biochim Biophys Acta 1830:4960–4973.

D′Amours D, Sallmann FR, Dixit VM, Poirier GG. 2001. Gain-of-function of poly (ADP-ribose) polymerase-1 upon cleavage by apoptotic proteases: Implications for apoptosis. J Cell Sci 114:3771–3778.

Dai M, Jin Y, Gallegos JR, Lu H. 2006. Balance of yin and yang: Ubiquitylation-mediated regulation of p53 and c-Myc. Neoplasia 8:630–644.

Davis ME, Chen Z, Shin DM. 2008. Nanoparticle therapeutics: An emerging treatment modality for cancer. Nat Rev Drug Discov 7:771–782.

Eblen ST. 2012. Regulation of chemoresistance via alternative messenger RNA splicing. Biochem Pharmacol 83:1063–1072.

El Sohaimy SA, Hamad GM, Mohamed SE, Amar MH, Al-Hindi RR. 2015. Biochemical and functional properties of *Moringa oleifera* leaves and their potential as a functional food. GARJAS 4:188–199.

Erasto P, Adebola PO, Grierson S, Afolayan AJ. 2005. An ethnobotanical study of plants used for the treatment of diabetes in the Eastern Cape Province, South Africa. African J Biotech 12:1458–1460.

Fahey JW. 2005. *Moringa oleifera*: A review of the medical evidence for its nutritional, therapeutic, and prophylactic properties. Part 1. Trees for Life J 1:1–15.

Fischer U, Schulze-Osthoff K. 2005. Apoptosis-based therapies and drug targets. Cell Death Diff 12:942–961.

Gao W, Xu K, Ji L, Tang B. 2011. Effect of gold nanoparticles on glutathione depletion-induced hydrogen peroxide generation and apoptosis in HL7702 cells. Toxicol Lett 205:86–95.

Garrido C, Brunet M, Didelot C, Zermati Y, Schmitt E, Kroemer G. 2006. Heat shock proteins 27 and 70 anti-apoptotic proteins with tumorigenic properties. Cell Cycle 5:2592–2601.

Globocan. 2012. Globocan 2012 Estimated Cancer Incidence, Mortality, Prevalence and Disability-Adjusted Life Years (DALYs) Worldwide in 2012 [http://globocan.iarc.fr/].

Goyal BR, Agrawal BB, Goyal RK, Mahta AA. 2007. Phyto-pharmacology of *Moringa oleifera* Lam an overview. Nat Prod Rad 6:347–353.

Hengartner MO. 2000. The biochemistry of apoptosis. Nature 407:770–776.

Ho JA, Chang H, Shih N, Wu L, Chang Y, Chen C, Chou C. 2010. Diagnostic detection of human lung cancer-associated antigen using a gold nanoparticle-based electrochemical immunosensor. Anal Chem 82:5944–5950.

Jeyaraj M, Arun R, Sathishkumar G, MubarakAli D, Rajesh M, Sivanandhan G, Kapildev G, Manickavasagam M, Thajuddin N, Ganapathi A. 2014. An evidence on G2/M arrest, DNA damage and caspase mediated apoptotic effect of biosynthesized gold nanoparticles on human cervical carcinoma cells (HeLa). Mater Res Bull 52:15–24.

Kang B, Mackey MA, El-Sayed M. 2010. Nuclear targeting of gold nanoparticles in cancer cells induces DNA damage, causing cytokinesis arrest and apoptosis. J Am Chem Soc 132:1517–1519.

Kim T, Kang JM, Hyun J, Lee B, Kim SJ, Yang E, Hong S, Lee H, Fujii M, Niederhuber JE, Kim S. 2014. The Smad7-Skp2 complex orchestrates Myc stability, impacting on the cytostatic effect of TGF-β. J Cell Sci 127:411–421.

Kotakadi VS, Gaddam SA, Rao YS, Prasad TNVKV, Reddy AV, Sai Gopal DVR. 2014. Biofabrication of silver nanoparticles using *Andrographis paniculata*. Eur J Med Chem 73:135–140.

Kumar A, Boruah BM, Liang X. 2011. Gold nanoparticles: Promising nanomaterials for the diagnosis of cancer and HIV/AIDS. J Nano 2011:1–17.

Leong DT, Ng KW. 2014. Probing the relevance of 3D cancer models in nanomedicine research. Adv Drug Deliv Rev 79–80:95–106.

Li D, Liu Z, Yuan Y, Liu Y, Niu F. 2015. Green synthesis of gallic acid-coated silver nanoparticles with high antimicrobial activity and low cytotoxicity to normal cells. Process Biochem 50:357–366.

Lim ZJ, Li JJ, NG C, Yung LL, Bay B. 2011. Gold nanoparticles in cancer therapy. Acta Pharmacol Sin 32:983–990.

Livak KJ, Schmittgen TD. 2001. Analysis of relative gene expression data using real-time quantitative PCR and the $2^{-\Delta\Delta Ct}$ method. Methods 25:402–408.

Luqman S, Srivastava S, Kumar R, Maurya AK, Chanda D. 2012. Experimental assessment of *Moringa oleifera* leaf and fruit for its antistress, antioxidant, and scavenging potential using in vitro and in vivo assays. Evid Based Complement Alternat Med 2012:1–12.

Manley JL, Krainer AR. 2010. A rational nomenclature for serine/arginine-rich protein splicing factors (SR proteins). Genes Dev 24:1073–1074.

Massiello A, Chalfant CE. 2006. SRp30a (ASF/SF2) regulates the alternative splicing of caspase-9 pre-mRNA and is required for ceramide-responsiveness. J Lipid Res 47:892–897.

Mendis S, Armstrong T, Bettcher D, Branca F, Lauer J, Mace C, Poznyak V, Riley L, Da Costa E, Silva V, Stevens G. 2014. Global status report on noncommunicable diseases 2014. WHO 1–280.

Mishra G, Singh P, Verma R, Kumar S, Srivastav S, Jha KK, Khosa RL. 2011. Traditional uses, phytochemistry and pharmacological properties of *Moringa oleifera* plant: An overview. Der Pharmacia Lettre 3:141–164.

Montazeri A, Milroy R, Hole D, McEwen J, Gillis CR. 2001. Quality of life in lung cancer patients as an important prognostic factor. Lung Cancer 31:233–240.

Mossman T. 1983. Rapid colorimetric assay for cellular growth and survival: Application to proliferation and cytotoxicity assay. J Immunol Methods 65:55–63.

Ndubuaku UM, Nwankwo VU, Baiyeri KP. 2013. Influence of poultry manure application on leaf amino acid profile, growth and yield of moringa (*Moringa oleifera* Lam) plants. Int J Cur Tr Res 2:390–396.

Parveen A, Roa S. 2014. Cytotoxicity and genotoxicity of biosynthesized gold and silver nanoparticles on human cancer cell lines. J Clust Sci 1–14.

Prasad TNVKV, Elumalai EK. 2011. Biofabrication of Ag nanoparticles using *Moringa oleifera* leaf extract and their antimicrobial activity. Asian Pac J Trop Biomed 439–442.

Roth E, Oehler R, Manhart N, Exner R, Wessner B, Strasser E, Spittler A. 2002. Regulative potential of glutamine-relation to glutathione metabolism. Nutrition 18:217–221.

Salamanca-Buentello F, Persad DL, Court EB, Martin DK, Daar AS, Singer PA. 2005. Nanotechnology and the developing world. PLoS Med 2:0383–0386.

Schlegel RA, Williamson P. 2001. Phosphatidylserine, a death knell. Cell Death Diff 8:551–563.

Selim M, Hendi A. 2012. Gold nanoparticles induce apoptosis in MCF-7 human breast cancer cells. A Pac J Can Prev 13:1617–1620.

Shankar SS, Rai A, Ankamwar B, Singh A, Ahmad A, Sastry M. 2004. Biological synthesis of triangular gold nanoprisms. Nature Mater 3:482–488.

Shultz JC, Goehe RW, Murudkar CS, Wijesinghe DS, Mayton EK, Massiello A, Hawkins AJ, Mukerjee P, Pinkerman RL, Park MA, Chalfant CE. 2011. SRSF1 regulates the alternative splicing of caspase 9 via a novel intronic splicing enhancer affecting the chemotherapeutic sensitivity of non-small cell lung cancer cells. Mol Cancer Res 9:889–900.

Shultz JC, Goehe RW, Wijesinghe DS, Murudkar C, Hawkins AJ, Shay JW, Minna JD, Chalfant CE. 2010. Alternative splicing of caspase 9 is modulated by the phosphoinositide 3-Kinase/Akt pathway via phosphorylation of SRp30a. Cancer Res 70:9185–9196.

Siddiqi NJ, Abdelhalim M, El-Ansary A, Alhomida AS, Ong W. 2012. Identification of potential biomarkers of gold nanoparticle toxicity in rat brains. J Neuro 9:1–16.

Sreelatha S, Jeyachitra A, Padma PR. 2011. Antiproliferation and induction of apoptosis by *Moringa oleifera* leaf extract on human cancer cells. Food Chem Toxicol 49:1270–1275.

Stuchinskaya T, Moreno M, Cook MJ, Edwards DR, Russell DA. 2011. Targeted photodynamic therapy of breast cancer cells using antibody-phthalocyanine-gold nanoparticle conjugates. Photochem Photobiol Sci 10:822–831.

Sukirtha R, Priyanka KM, Antony JJ, Kamalakkannan S, Thangam R, Gunasekaran P, Krishnan M, Achiraman S. 2012. Cytotoxic effect of green synthesized silver nanoparticles using *Melia azedarach a*gainst in vitro HeLa cell lines and lymphoma mice model. Process Biochem 47:273–279.

Tay CY, Setyawati MI, Xie J, Parak WJ, Leong DT. 2014. Back to basics: Exploiting the innate physico-chemical characteristics of nanomaterials for biomedical applications. Adv Funct Mater 24:5936–5955.

Tedesco S, Doyle H, Blasco J, Redmond G, Sheehan D. 2010. Oxidative stress and toxicity of gold nanoparticles in Mytilus edulis. Aquatic Toxicol 100:178–186.

Tiloke C, Phulukdaree A, Chuturgoon AA. 2013. The antiproliferative effect of *Moringa oleifera* crude aqueous leaf extract on cancerous human alveolar epithelial cells. BMC Complement Altern Med 13:1–8.

Wang X. 2001. The expanding role of mitochondria in apoptosis. Genes Dev 15:2922–2933.

Wilson K, Walker J. 2005. Principles and techniques of biochemistry and molecular biology. England: Cambridge University Press.

Xie J, Lee JY, Wang DIC. 2007a. Synthesis of single-crystalline gold nanoplates in aqueous solutions through biomineralization by serum albumin protein. J Phys Chem C 111:10226–10232.

Xie J, Lee JY, Wang DIC, Ting YP. 2007b. Identification of active biomolecules in the high-yield synthesis of single-crystalline gold nanoplates in algal solutions. Small 3:672–682.

Xie J, Lee JY, Wang DIC, Ting YP. 2007c. Silver nanoplates: From biological to biomimetic synthesis. ACS Nano 1:429–439.

Xie J, Zheng Y, Ying JY. 2009. Protein-directed synthesis of highly fluorescent gold nanoclusters. J Am Chem Soc 131:888–889.

Yang Y, Ma H. 2009. Western blotting and ELISA techniques. Researcher 1:67–86.

Zhang P, Gao WY, Turner S, Ducatman BS. 2003. Gleevec (STI-571) inhibits lung cancer cell growth (A549) and potentiates the cisplatin effect in vitro. BMC Mol Cancer 2:1–9.